THE JOURNAL OF PHYSICAL CHEMISTRY B

Article

pubs.acs.org/JPCB

Effects of Hydrogen Bonding on Internal Conversion of GFP-like Chromophores. II. The *meta*-Amino Systems

Chi-Wen Cheng,[‡] Guan-Jhih Huang,[†] Hung-Yu Hsu,[‡] Ch. Prabhakar,[†] Yuan-Pern Lee,*[,‡,§] Eric Wei-Guang Diau,*[,‡] and Jye-Shane Yang*[,†]

[†]Department of Chemistry, National Taiwan University, Taipei 10617, Taiwan

[‡]Department of Applied Chemistry and Institute of Molecular Science, National Chiao Tung University, Hsinchu 30010, Taiwan

[§]Institute of Atomic and Molecular Sciences, Academia Sinica, Taipei 10617, Taiwan

Supporting Information

ABSTRACT: To rationalize the efficient quenching of the fluorescence and the $Z \rightarrow E$ photoisomerization of *m*-ABDI, the *meta*-amino analogue of the green fluorescent protein (GFP) chromophore, in protic solvents, the femtosecond time-resolved fluorescence and transient infrared (TRIR) spectra of *m*-ABDI in CD_3CN, CH_3OH, and CD_3OD are determined. For solutions in CD_3CN, the fluorescence decay lifetime is ~7.9 ns and IR absorption lines near 1513, 1531, 1557, and 1613 cm^{-1} of *m*-ABDI in its electronically excited state were observed with a decay time >5 ns. For solutions in CH_3OH, the fluorescence decay is double exponential with time constants of ~16 and 62 ps. In addition to IR absorption lines of *m*-ABDI in its electronically excited state with a decay time of ~16 ps, new features near 1513, 1532, 1554, and 1592 cm^{-1} were observed to have a rise time of ~19 ps and a decay constant of ~58 ps, indicating formation of an intermediate. The assignments for the IR spectra of the ground and excited states were assisted with DFT and TDDFT calculations, respectively. We conclude that the torsion of the exocyclic C═C bond (the τ torsion) is responsible for the nonradiative decay of electronically excited *m*-ABDI in CD_3CN. However, in CH_3OH and CD_3OD, the solute−solvent hydrogen bonding (SSHB) interactions diminish significantly the barrier of the τ torsion and induce a new pathway that competes successfully with the τ torsion, consistent with the efficient fluorescence quenching and the diminished yield for $Z \rightarrow E$ photoisomerization. The new pathway is likely associated with excited-state proton transfer (ESPT) from the solvent to *m*-ABDI, particularly the carbonyl group, and generates an intermediate (ESPT*) that is weakly fluorescent.

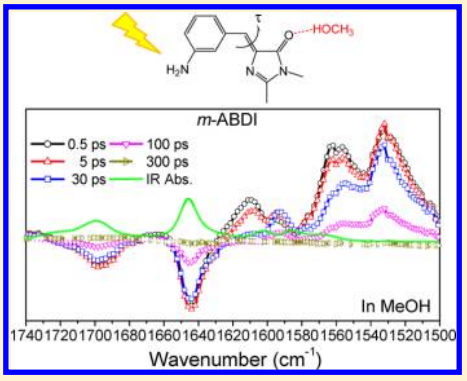

INTRODUCTION

The phenomenon of enhanced photochemical reactivity for *meta*- vs *para*-substituted systems is often termed the "*meta* effect".[1−3] Zimmerman devised this term to account for the solvolytic activity of a number of *meta*-disubstituted benzenes in their excited states enhanced relative to the corresponding *para*-disubstituted benzenes, which is of the reverse for the ground-state reactivity.[1] The *meta* effect has been demonstrated with other photochemical properties.[4,5] One particular example is the *meta*-amino effect on the enhancement of fluorescence quantum efficiency (Φ_f) of *trans*-stilbenes; in cyclohexane, Φ_f (0.78) of *trans*-3-aminostilbene is 15 times that (0.05) of *trans*-4-aminostilbene.[6] The *meta*-amino effect originates from an increased barrier height for the torsion of the C═C bond in the lowest singlet excited state so that the fluorescence decay becomes kinetically favored.

The great utility of the green fluorescent protein (GFP) as a biomarker[7−10] has inspired much research on GFP-like chromophores both to understand the structure−property relationship and for applications as fluorescent probes[11] or light-emitting materials.[12,13] It is well-documented that the parent GFP chromophore, *p*-hydroxybenzylidenedimethylimidazolinone (*p*-HBDI), is nearly nonemissive ($\Phi_f < 10^{-3}$) in nonviscous solutions at ambient temperature.[14,15] The ultrafast fluorescence quenching is associated with the torsion of the exocyclic C═C bond (the τ torsion).[16−18] Effective suppression of this τ torsion is thus a prerequisite to creation of GFP-like chromophores of large Φ_f. Whereas this can be readily achieved with covalent linking of the two aromatic rings that constrains the τ torsion,[19,20] most unconstrained GFP-like chromophores are weakly fluorescent with Φ_f lower than 0.10.[21−25]

One of our laboratories recently reported that the *meta*-amino effect on enhanced fluorescence applies also to the GFP chromophore. The *meta*-amino derivative *m*-ABDI (Chart 1) exhibits Φ_f as large as 0.34 in hexane, which is more than 100 times that of the *para* isomer *p*-ABDI ($\Phi_f < 10^{-3}$).[16] In contrast, the fluorescence is nearly quenched and the quantum yield of $Z \rightarrow E$ isomerization (Φ_{ZE}) is greatly diminished in protic solvents, such as CH_3OH, indicating a significant solute−

Received: September 20, 2012
Revised: January 29, 2013
Published: February 12, 2013

   dx.doi.org/10.1021/jp3093397 | *J. Phys. Chem. B* 2013, 117, 2705−2716

solvent hydrogen bonding (SSHB) effect on the decay dynamics. To characterize the fluorescence-quenching SSHB effect, we have measured the femtosecond fluorescence decay and time-resolved infrared (TRIR) spectra of both *p*-ABDI and *m*-ABDI in selected solvents. In the preceding paper, the excited-state dynamics of *p*-ABDI were discussed;[26] we report here the results for *m*-ABDI. We conclude that the nonradiative decay of *m*-ABDI in aprotic solvents is dominated by the τ torsion, whereas in protic solvents the SSHB opens new channels for internal conversion (IC). According to calculations of the time-dependent density functional theory (TDDFT) on the IR absorption of *m*-ABDI in the excited state, the IC channel might be coupled with a proton transfer from the solvent molecule to the carbonyl oxygen of *m*-ABDI in the excited state. The SSHB effect on the τ torsion is also discussed.

Chart 1

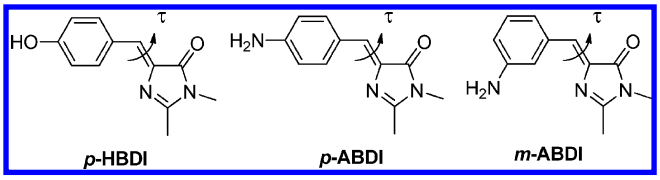

EXPERIMENTAL SECTION

The synthesis and X-ray crystal structure of *m*-ABDI have been reported.[16] The steady-state and femtosecond time-resolved instruments and experimental methods are the same as those described for *p*-ABDI in the preceding paper.[26] The ^{1}H NMR spectra of both the *Z* and *E* isomers of *m*-ABDI in DMSO-d_6 and HPLC chromatograms of *m*-ABDI before and after irradiation are shown in Figure S1 (Supporting Information).

Picosecond Time-Resolved Measurements. Picosecond temporally resolved spectra were obtained with a time-correlated single-photon counting (TCSPC) system (Fluotime 200, PicoQuant). The excitation source was provided by a 400 nm pulsed-diode laser (LDH-400, PicoQuant), which was controlled by a pulsed laser driver (PDL800-D, PicoQuant). The excitation laser was focused onto the sample holder by a lens. A lens collected fluorescence emitted from the sample at a right angle. An iris was used to attenuate the intensity of the detected signal, and the polarization of the detected fluorescence relative to the excitation laser pulse was set at 54.7° (magic angle) with a polarizer. A subtractive double monochromator (9030DS, Sciencetech) compensated the GVD of fluorescence and selected the detection wavelength. A multichannel plate photomultiplier (R3809U, Hamamatsu) was connected to a computer with a TCSPC-module (SPC-630, Becker and Hickl) card for data acquisition.

Data Analysis of TRIR Spectra. For the quantitative analysis of TRIR data for *m*-ABDI in selected solvents, we performed the global and target analysis by using the GLOTARAN software package.[27,28] The aim of the analysis is to obtain a model-based description of the time-resolved data in terms of a small number of precisely estimated rate constants and difference spectra so as to elucidate a photoinduced process in complex systems. The global analysis performs a simultaneous analysis using a model of sequential reactions. In this program, all TRIR spectra are collected in a matrix, which was globally fitted by applying a sequential kinetic scheme with increasing lifetimes. In this work, the time-resolved difference spectra were fitted with two kinetic models. A parallel model

$$A \xrightarrow{k_1}, B \xrightarrow{k_2}, C \xrightarrow{k_3}$$

of independently decaying components yielded decay associated difference spectrum (DADS), which represent the decay of spectra associated with varied species with distinct lifetimes upon photoexcitation. The sequential model

$$A \xrightarrow{k_1} B \xrightarrow{k_2} C$$

yields evolution associated difference spectra (EADS), which represent spectral evolution that is associated with the temporal behavior of each species. The target analysis applied a particular kinetic model to fit the observed TRIR data. We tried the model

$$A \xrightarrow{k_1} B \xrightarrow{k_2} C, A \xrightarrow{k_3} C$$

and found that converged results could be obtained only when k_1 or k_3 is fixed, and the resultant $k_1 + k_3$ is identical to the k_1 in the sequential model

$$A \xrightarrow{k_1} B \xrightarrow{k_2} C$$

Calculations. All the calculations were carried out using the Gaussian 09 package.[29] The electronic ground- and excited-state geometry optimizations adopted the density functional theory (DFT) and time-dependent density functional theory (TDDFT) methods, respectively. Becke's three-parameter hybrid exchange functional and the Lee–Yang–Parr correlation functional (B3LYP)[30,31] were utilized in the calculation with a 6-31G* basis set. Vibrational frequencies were evaluated for the optimized geometries at the same level to ensure that the structure obtained was a minimum on the potential energy surface. The polarizable continuum model (PCM)[32] was employed for the bulk solvent effects with the solvents CH_3CN (dielectric constant, ε = 35.688) and CH_3OH (dielectric constant, ε = 32.613). The geometric optimizations of the hydrogen-bonded *m*-ABDI–CH_3OH complexes were considered here as one and two methanol molecules with *m*-ABDI in the ground and excited states. The IR intensities were determined from the gradients of the dipole moment. All the calculated vibrational frequencies are scaled by a factor of 0.96 to correct the anharmonicity effects.[33−35] To predict the absorption maxima, vertical excitation energies were calculated at the ground-state geometry with the time-dependent DFT (TDDFT) method at the B3LYP/6-31G** level.

RESULTS AND DISCUSSION

Steady-State Electronic Spectra. The UV–vis absorption and emission spectra of *m*-ABDI in hexane, THF, CH_3CN, and CH_3OH are shown in Figure 1. The absorption spectra depend only slightly on the solvent. For example, the absorption maximum (λ_{abs}) of *m*-ABDI was bathochromically shifted by ~400 cm^{-1} when hexane was replaced by CH_3OH, but the corresponding solvatochromic shift was ~1900 cm^{-1} for the *para* isomer *p*-ABDI.[26] The small solvent effect in the *meta* systems is attributed to the inherently weaker mesomeric interactions between the amino donor and the imidazolinone acceptor. In contrast, the fluorescence maximum (λ_f) exhibits a large solvatochromic shift (5431 cm^{-1}) on proceeding from hexane to CH_3OH, indicating that the lowest excited state (S_1) is highly polarized. For comparison, the corresponding

dx.doi.org/10.1021/jp3093397 | J. Phys. Chem. B 2013, 117, 2705−2716

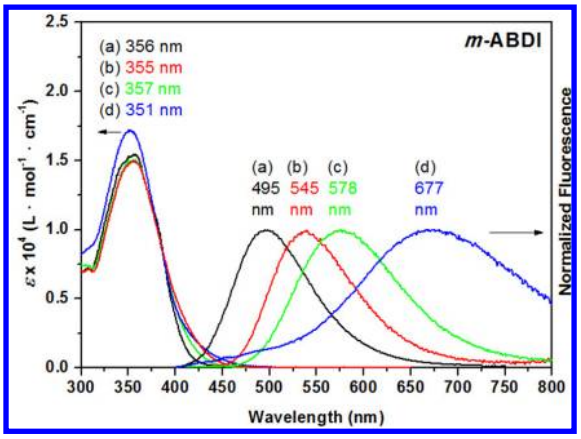

Figure 1. Absorption (left) and fluorescence spectra (right) of *m*-ABDI in (a) hexane, (b) THF, (c) CH_3CN, and (d) CH_3OH at 296 K.

solvatofluorochromic shift for *p*-ABDI is 2466 cm^{-1}. Evidently, the excited state of *m*-ABDI possesses a larger extent of charge separation than that of *p*-ABDI, which is again due to weaker mesomeric interactions between the donor and acceptor groups after photoinduced charge transfer. It should also be noted that the spectrum in CH_3OH shows dual fluorescence. The short-wavelength band near 495 nm is similar to that in hexane and the intensity is much weaker than the long-wavelength band at 677 nm. According to the femtosecond fluorescence and IR transients (*vide infra*), the short- and long-wavelength emissions result from *m*-ABDI and a protonated intermediate, respectively, in the excited state.

The electronic structure of *m*-ABDI in the gas phase with the geometry optimized at the B3LYP/6-31G* level was investigated with TDDFT calculations at the TD-B3LYP/6-31G** level. The benzylideneimidazolinone moiety is planar in the optimized structure, consistent with the reported X-ray crystal structure for *m*-ABDI, in which the dihedral angle defined by the phenyl and imidazolinone rings is only 5.1°.[16] Two distinct conformers, *syn* and *anti*, depend on the relative orientation of the NH_2 and C═O groups. The *anti* form is more stable than the *syn* form by ∼0.5 kcal mol^{-1} in the gas phase (Table S1, Supporting Information), but only the *syn* form was observed in the solid state according to the X-ray crystal structure.[16] The calculated absorption wavelength ($\lambda_{max,cal}$) and oscillator strength (f) agree satisfactorily with the observed spectra (Table S2, Supporting Information). The lowest energy transition $S_0 \rightarrow S_1$ near 395 nm is weak ($f < 0.1$), and the more intense transitions are at higher energies with f being 0.30 and 0.20, respectively, for the nearly degenerate $S_0 \rightarrow S_2$ and $S_0 \rightarrow S_3$ transitions near 342 nm. The HOMO → LUMO is the major configuration of the S_1 state. As shown in Figure 2, the probability of finding electrons in the amino group is negligible in the LUMO but significant in the HOMO. The

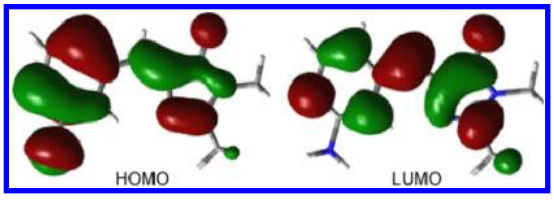

Figure 2. Frontier molecular orbitals of *m*-ABDI calculated at the B3LYP/6-31G** level.

S_1 state thus possesses a charge-transfer character. In contrast, the S_2 and S_3 states are more localized in the benzylideneimidazolinone moiety. The large solvatofluorochromic shift from hexane to CH_3CN is consistent with a charge-transfer S_1 state.

The prediction of a low-intensity transition to the charge-transfer S_1 state and a more intense one to the localized S_2 state for *m*-ABDI is reminiscent of *trans*-3-aminostilbene (*m*-AS) and its derivative *trans*-3-(*N*,*N*-dimethylamino)stilbene (*m*-DS).[6,36] The S_1-S_2 energy gaps estimated from the absorption spectra in methylcyclohexane are 3162 and 4317 cm^{-1} for *m*-AS and *m*-DS, respectively. The increase in the S_1-S_2 gap on going from *m*-AS to *m*-DS reflects the enhanced charge-transfer character of the chromophores. Along with the increase in the S_1-S_2 gap is a decrease in the intensity of the $S_0 \rightarrow S_1$ absorption band, indicating the occurrence of intensity borrowing from the higher excited states of more allowed transition. This phenomenon was also observed for *m*-ABDI and its dimethylamino derivative *m*-DMABDI.[37] Whereas there is no distinct band but a small tailing that corresponds to the weak $S_0 \rightarrow S_1$ transition in the absorption spectra of *m*-ABDI, a low-lying shoulder near 420 nm that is distinct from the intense band near 350 nm is present for *m*-DMABDI. It is anticipated that the S_1-S_2 gap could be further enlarged in the excited state because of the enhanced charge-transfer character of the S_1 state, and thus, the rate of the $S_1 \rightarrow S_0$ emission is reduced. This argument is supported by the long fluorescence lifetimes for all these *meta* systems (*vide infra*).

Quantum Yields. The Φ_f values of *m*-ABDI in hexane (0.34), THF (0.28), CH_3CN (0.16), and CH_3OH ($<10^{-3}$) at 296 K have been reported.[16] Compared with other unconstrained GFP-like chromophores, the Φ_f of *m*-ABDI in the aprotic solvents is unusually high as a result of the *meta*-amino effect.[4−6] The Φ_f decreases with increasing solvent polarity from hexane to CH_3CN. However, the behavior is different in CH_3OH, in which the fluorescence is nearly quenched.

The Φ_{ZE} values of *m*-ABDI in hexane (0.37), THF (0.35), CH_3CN (0.45), and CH_3OH (0.08) were also reported.[16] We have previously proposed that the parameter $\Phi_f + 2\Phi_{ZE}$ or $\Phi_f + 2\Phi_{EZ}$ is a useful probe to study the decay channels of alkenes of *E*,*Z*-photoisomerization activity.[6,23,38−40] This proposition stems from the one-bond-flip (OBF) mechanism of photoisomerization,[16,23,41] in which IC occurs at the perpendicular state $^1p^*$ with an ∼90° torsion of the C═C bond so that the probability of forming the *E* and *Z* isomers is ∼50% for each. This condition corresponds to a quantum yield $2\Phi_{ZE}$ and $2\Phi_{EZ}$ for the C═C torsion in the *Z* and *E* isomers, respectively. For *m*-ABDI, the moderate magnitude of Φ_f and that $\Phi_f + 2\Phi_{ZE} \cong 1.0$ in aprotic solvents indicate that fluorescence and the τ torsion are responsible for the deactivation of the excited state. The increase in Φ_{ZE} at the expense of Φ_f in more polar solvents reveals a solvent effect on the barrier of τ torsion, which is decreased in more polar solvents. In CH_3OH, the Φ_f becomes negligible and $2\Phi_{ZE}$ is much less than 1.0. This condition indicates the presence of a new nonradiative decay channel that is induced by the SSHB interactions; such an indication is supported by the time-resolved fluorescence and IR spectra (*vide infra*).

Steady-State IR Spectra. The IR spectra of *m*-ABDI in its electronic ground state in CD_3CN, CH_3OH, and CD_3OD in the spectral region 1500−1750 cm^{-1} are shown in Figure 3; the intensity is normalized to absorption near 1650 cm^{-1}. The spectra can be deconvoluted into six major vibrational bands (Figure S2, Supporting Information), and the wavenumbers

dx.doi.org/10.1021/jp3093397 | J. Phys. Chem. B 2013, 117, 2705−2716

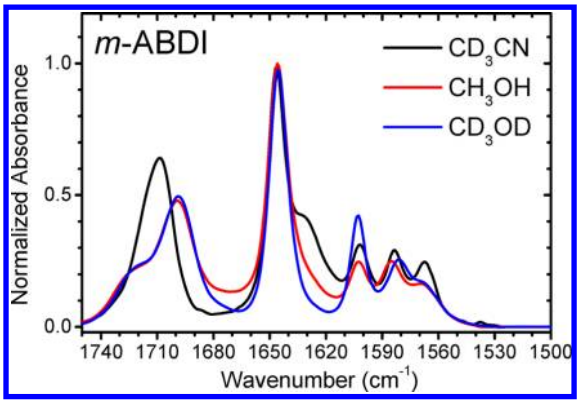

Figure 3. Normalized IR spectra in the region 1500−1750 cm^{-1} for *m*-ABDI in CD_3CN, CH_3OH, and CD_3OD.

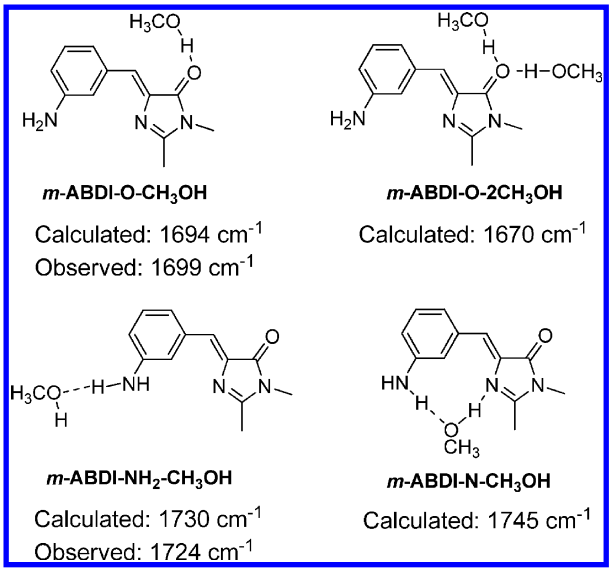

Figure 4. Schematic illustration of possible hydrogen bonding of *m*-ABDI in CH_3OH and the calculated vibration frequency for the C═O stretching mode.

and relative amplitudes of these bands are summarized in Table 1, with their assignments according to DFT calculations at the B3LYP/6-31G* level of theory (Figure S3, Supporting Information). The calculated wavenumbers and relative intensities agree satisfactorily with the observed spectra. The intense band near 1650 cm^{-1} corresponds to the exocyclic C═C bond stretching coupled with the C═N stretching and the NH_2 bending. The band near 1570 cm^{-1} is associated with the phenyl stretching coupled with the exocyclic C═C and C═N stretching modes. The bands at 1585 and 1600 cm^{-1} correlate with the phenyl stretching coupled with the C═N stretching and NH_2 bending modes. The shoulder at 1630 cm^{-1} in CD_3CN is ascribed to the NH_2 bending, but the corresponding band in CH_3OH and CD_3OD might be overlapped with the band at ∼1650 cm^{-1}. Finally, the broad band at ∼1710 cm^{-1} is associated with the C═O stretching mode. This band splits into two bands near 1700 and 1725 cm^{-1} in both CH_3OH and CD_3OD as a consequence of SSHB interactions. A splitting of the C═O absorption band in protic solvents was also observed for *p*-ABDI[26] and other organic dyes with carbonyl groups.[42−44]

DFT calculations on several SSHB modes (Figure 4) between *m*-ABDI and CH_3OH molecules were performed to gain insight into the observed SSHB-induced shift of the C═O stretching band. The calculated vibrational modes are shown in Figure S4−S7 (Supporting Information), and the data are listed in Table S3 (Supporting Information). The results indicate that the IR absorptions at ∼1700 and 1725 cm^{-1} correspond to a HB between CH_3OH and the carbonyl oxygen (*m*-ABDI—O—CH_3OH) and between the amino hydrogen and the oxygen of CH_3OH (*m*-ABDI—NH_2—CH_3OH), respectively. More HBs to the carbonyl oxygen (e.g., *m*-ABDI—O—$2CH_3OH$) would further lower the C═O stretching frequency, and HB to both the amino and imino nitrogen (e.g., *m*-ABDI—N—CH_3OH) would further increase the C═O stretching frequency.

Time-Resolved Fluorescence Profiles. Fluorescence lifetimes (τ_f) of *m*-ABDI in CD_3CN and CH_3OH at 296 K were measured with time-correlated single photon counting (TCSPC). The fluorescence decay profile of *m*-ABDI in CD_3CN is fitted well with a single exponential function,

Table 1. Experimental and Calculated Wavenumbers and Relative Intensities of the Vibration Bands in the Region 1500−1750 cm^{-1} for *m*-ABDI in CD_3CN, CH_3OH, and CD_3OD[a]

	wavenumber (cm^{-1})				mode description
mode	CD_3CN	CH_3OH	CD_3OD	caln[b]	phenyl (Ph), stretch (S), bend (B), exocyclic (e-)
ν_{63}	1568	1568	1568	1558	Ph (S) + C═C (e-S) + C═N (S)
	(29)	(19)	(28)	(17)	
ν_{64}	1583	1584	1582	1570	Ph (S) + C═N (S) + NH_2 (B)
	(27)	(16)	(26)	(10)	
ν_{65}	1602	1603	1603	1593	Ph (S) + C═N (S) + NH_2 (B)
	(34)	(28)	(33)	(11)	
ν_{66}	1630	u.r.[c]	u.r.[c]	1626	NH_2 (B)
	(77)			(24)	
ν_{67}	1646	1645	1645	1637	C═C (e-S) + C═N (S) + NH_2 (B)
	(100)	(100)	(100)	(100)	
ν_{68}	1710	1699	1699	1733	C═O (S)
	(143)	(80)	(85)	(73)	
ν_{69}[d]		1724	1721		C═O (S)
		(22)	(40)		

[a]Relative intensities normalized to the absorption band near 1645 cm^{-1} are listed in parentheses. [b]Vibrational wavenumbers calculated with B3LYP/6-31G* in the gas phase are scaled by 0.96. [c]u.r. = unresolved bands. [d]Additional vibrational band split from ν_{68} due to SSHB.

dx.doi.org/10.1021/jp3093397 | J. Phys. Chem. B 2013, 117, 2705−2716

corresponding to a lifetime of 7.9 ns with excitation at 400 nm and detection at 600 nm (Figure S8, Supporting Information). The fluorescence decay of *m*-ABDI in CH_3OH was, however, much faster and unattainable with this technique because of the instrument response time 150 ps of TCSPC. Such a solvent effect on τ_f is consistent with the relative Φ_f determined in the two solvents.

To resolve the excited-state dynamics of *m*-ABDI in CH_3OH, the temporal profiles were investigated further with femtosecond fluorescence up-conversion. Figure 5 shows the

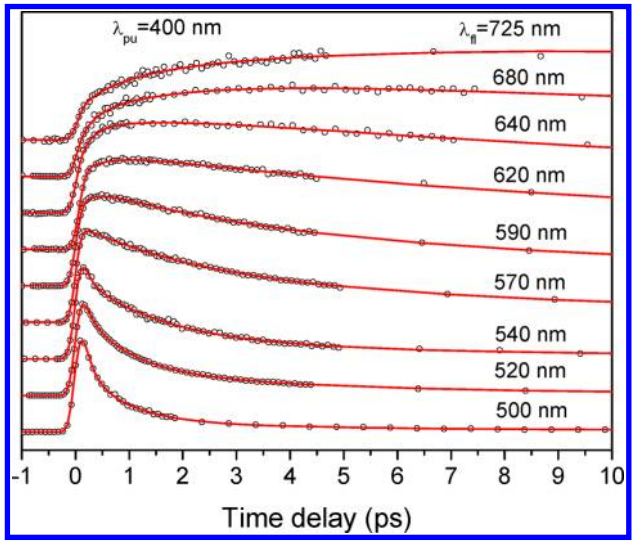

Figure 5. Normalized femtosecond-resolved fluorescence transients of *m*-ABDI in CH_3OH detected at indicated wavelengths.

fluorescence transients at a series of emission wavelengths from 500 to 725 nm. The fluorescence transients exhibit a rapid decay feature in the short-wavelength region and a rising feature to a plateau in the long-wavelength region, which is characteristic of solvation dynamics for an organic solute in a polar solvent. A plot of fluorescence intensity at 725 nm as a function of time (Figure S9, Supporting Information) shows a rise that exhibits a maximum near 10 ps; at 725 nm, the solvation has little effect on the temporal profile. A satisfactory fit of the plot requires three rising components (0.1 ± 0.2, 0.8 ± 0.3, and 5.2 ± 1.0 ps) and one decay component (55 ± 2 ps).

The wavelength-dependent fluorescence transients of *m*-ABDI in CH_3OH were converted to a time-resolved frequency plot (Figure S10, Supporting Information) according to a standard procedure.[45−48] The emission maximum at 508 nm (19667 cm^{-1}) in CH_3OH at time zero is near that at 495 nm (20202 cm^{-1}) in hexane. The emission maximum shifted to 700 nm (14500 cm^{-1}) after ∼12 ps. The solvation dynamics can be described by three decay components (0.15 ± 0.01, 1.26 ± 0.02, and 8.8 ± 0.1 ps), which are consistent with the results (multiple exponential decays with the average response time coefficient 5.0 ps) reported for Coumarin 153 in CH_3OH.[49] We constructed the time-resolved emission spectra (TRES) accordingly, and the results are shown in Figure S11 (Supporting Information). The TRES show the spectral shift toward low-energy region from 0.2 to 31.5 ps. After 30 ps, the spectra of the TRES show no significant change and the decays of the spectral intensities were mainly due to population loss in the excited state. We also estimated the total intensity by fitting the fluorescence spectra to an equation with the parameters width, height, and asymmetry factor.[50] The estimated total intensity involves a large uncertainty in the first 2 ps (Figure 6).

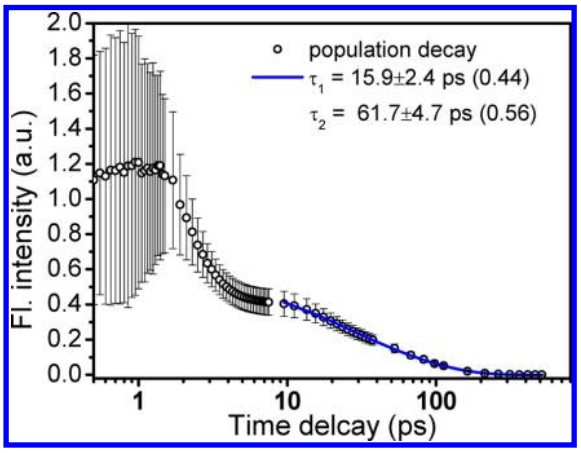

Figure 6. Time-dependent total intensity decay plot of *m*-ABDI in CH_3OH. The decay after 10 ps is fitted to two constants 16 and 62 ps, as shown with the blue line. Error bars for the data are shown.

The fluorescence decays rapidly for 2−10 ps. Because of the large uncertainties in the initial stage, we fitted data after 10 ps to a biexponential decay with time constants of 16 and 62 ps. The biexponential decays were tentatively assigned to two emissive species with different excited-state lifetimes detailed in the last section. Because of the complexity of the fluorescence transient spectra involving solvation, it is difficult to deconvolute the TRES shown in Figure S11 (Supporting Information) into two components as two emissive species in the excited state, but the trend of spectral shift can be easily identified.

Time-Resolved Infrared Spectra. The two-dimensional contour plots of the time-resolved infrared (TRIR) difference spectra in the spectral ranges 1500−1740 cm^{-1} (in CD_3CN and CH_3OH) and 1360−1740 cm^{-1} (CD_3OD) and in the time domains 0−1300 ps (CD_3CN), 0−300 ps (CH_3OH), and 0−800 ps (CD_3OD) for *m*-ABDI excited at 400 nm are shown in Figure 7a; positive values indicate formation, and negative values indicate depletion. The inverted ground-state IR absorption spectra are also shown in green in Figure 7a for comparison. The spectral region was extended to 1360 cm^{-1} for samples in CD_3OD because of less interference from the solvent. The difference spectra recorded at 0.5, 23, 103, 503, and 1403 ps in CD_3CN and at 0.5, 5.0, 30, 100, and 300 ps in CH_3OH and CD_3OD are shown in Figure 7b. In all three solvents, the ground-state absorption bands near 1650 and 1700 cm^{-1} are diminished (negative signals) upon irradiation. In addition, several positive features of transient absorption (TA), which depend on the solvent, appear in the region 1630−1500 cm^{-1}. Figure 7c shows the temporal profiles of TA signals at selected wavenumbers.

We performed global analysis[28,51] on the time-resolved difference spectra observed upon photoexcitation of *m*-ABDI in each solvent. For *m*-ABDI in CD_3CN, the data can be fitted with a single exponential decay and the DADS is shown in Figure 8a, with the associated decay curve presented in Figure 8b; the ground-state IR absorption spectra (green) are presented for comparison. The negative features are due to ground-state depletion, and the positive features are due to absorption of a new species (or state) upon photoexcitation. The ground-state recovery and the decay of new features were

dx.doi.org/10.1021/jp3093397 | J. Phys. Chem. B 2013, 117, 2705−2716

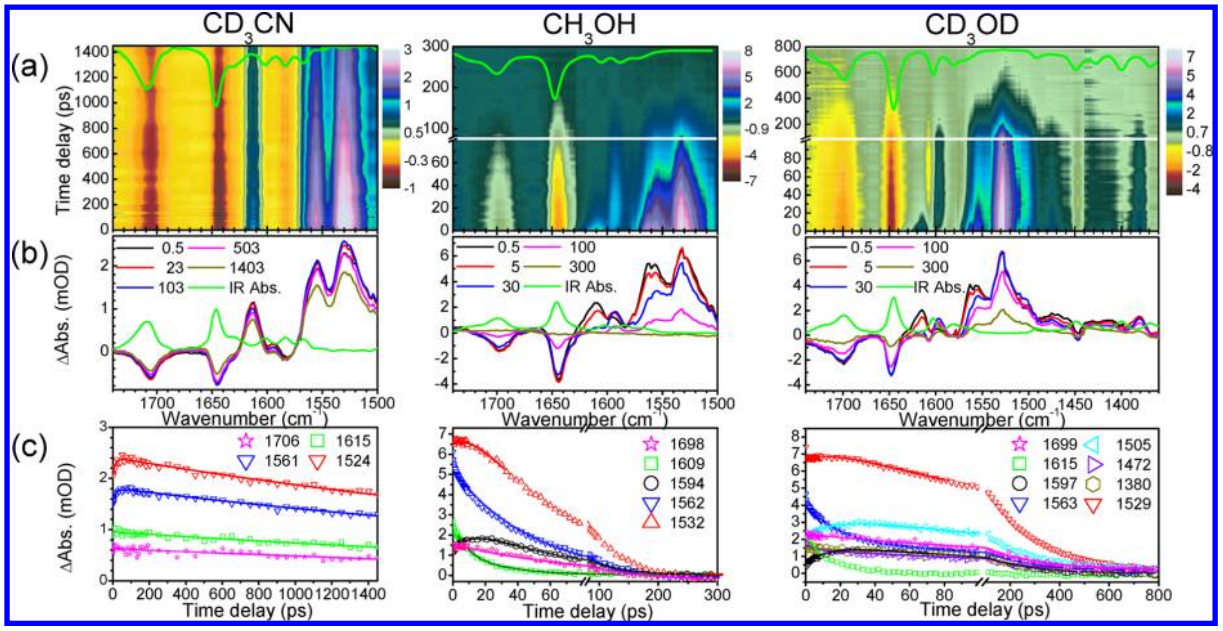

Figure 7. (a) Two-dimensional (wavenumber−time) TRIR spectra of *m*-ABDI in CD_3CN, CH_3OH, and CD_3OD upon 400 nm excitation. The ground-state IR absorption spectra (green) are presented for comparison in part a. (b) TRIR spectra recorded at 0.5, 23, 103, 503, and 1403 ps in CD_3CN and at 0.5, 5.0, 30, 100, and 300 ps in CH_3OH and CD_3OD. (c) Temporal profiles monitored at maxima of representative absorption bands. The intensity of the bleached signals at ~1700 cm^{-1} is multiplied by −1 for comparison.

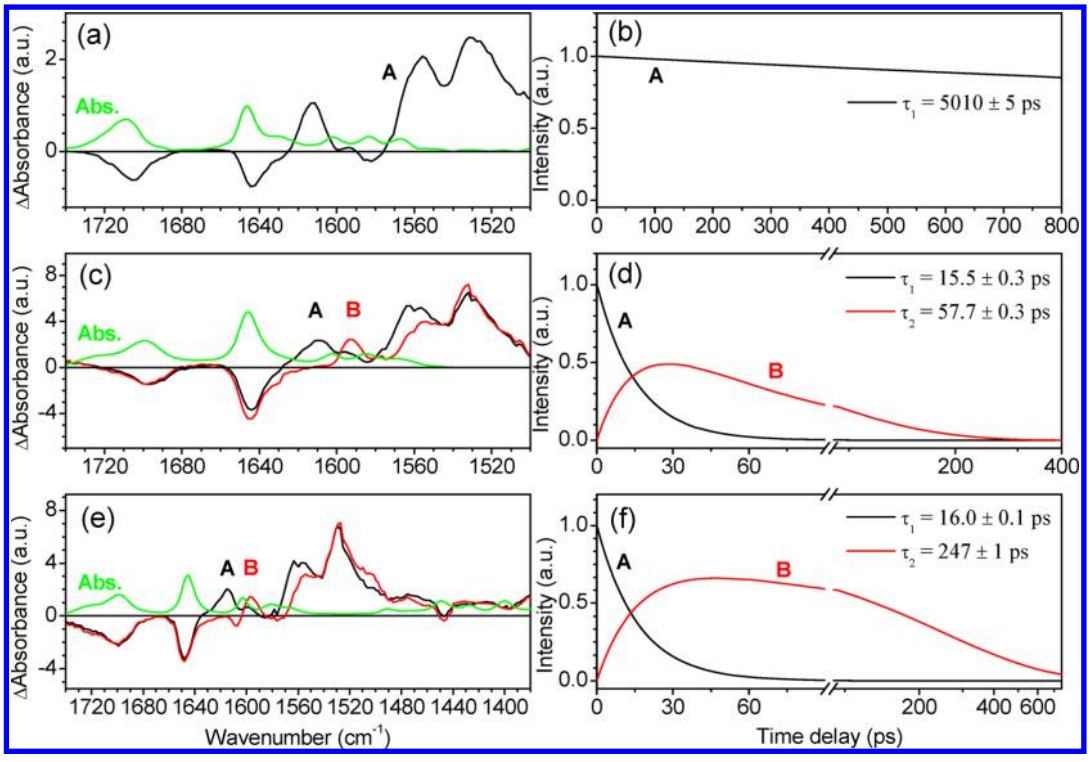

Figure 8. Evolution associated difference spectra (EADS) and concentration profiles obtained from the global analysis of *m*-ABDI in CD_3CN (a and b), CH_3OH (c and d), and CD_3OD (e and f). The ground-state IR absorption spectra (green) are presented for comparison.

fitted satisfactorily with a single exponential decay constant of 5.0 ns; this time constant might be smaller than the actual value because we only probed the absorption with a maximal delay of 1.5 ns. The decay constant of $\tau > 5.0$ ns for the new features is consistent with the observed fluorescence lifetime of 7.9 ns. For *m*-ABDI in CH_3OH, the observed spectra were fitted satisfactorily only with a sequential model

$$A \xrightarrow{k_1} B \xrightarrow{k_2} C$$

with $k_1 = 15.5 \pm 0.3$ ps and $k_2 = 57.7 \pm 0.3$ ps. The same sequential model was also applicable to *m*-ABDI in CD_3OD, and time constants of $k_1 = 16.0 \pm 0.1$ ps and $k_2 = 247 \pm 1$ ps were obtained. This is conceivable, as we observed a clear rise and decay for the feature near 1594 cm^{-1} (Figure 7c) and an isosbestic-like point near 1598 cm^{-1} in CH_3OH and near 1605

dx.doi.org/10.1021/jp3093397 | J. Phys. Chem. B 2013, 117, 2705−2716

Table 2. Experimental and Calculated Wavenumbers (cm^{-1}) and Relative Intensities of the Transient Excited-State Vibration Bands in the Region 1450−1750 cm^{-1} for *m*-ABDI and *m*-ABDI−OH^+ in CD_3CN, CH_3OH, and CD_3OD

mode	observed in CD_3CN[a]	calculation[b] *m*-ABDI in CH_3CN	mode description phenyl (Ph), stretch (S), bend (B), exocyclic (e-)
Species A			
ν_{63}	n.d.[c]	1494 (27)	C═N (S) + C—CH_3 (B) + N—CH_3 (B)
ν_{64}	1513 ± 13 (51)	1507 (100)	Ph (S)
ν_{65}	1531 ± 5 (100)	1512 (53)	Ph (S) + C═C (e-S)
ν_{66}	1557 ± 1 (74)	1557 (53)	C═C (e-S) + Ph (S)
ν_{67}	n.d.[c]	1616 (2)	NH_2 (B)
ν_{68}	1613 ± 1 (27)	1624 (68)	NH_2 (B) + C═O (S)

	in CH_3OH[a]	in CD_3OD[a]	*m*-ABDI in CH_3OH	
ν_{63}	n.d.[c]	1500 ± 9 (31)	1494 (26)	C═N (S) + C–CH_3 (B) + N—CH_3 (B)
ν_{64}	1512 ± 4 (33)	1515 ± 3 (37)	1507 (100)	phenyl (S)
ν_{65}	1531 ± 3 (100)	1530 ± 2 (100)	1512 (51)	C═C (e-S) + Ph (S)
ν_{66}	1560 ± 2 (103)	1557 ± 1 (100)	1557 (53)	C═C (e-S) + Ph (S)
ν_{67}	n.d.[c]	n.d.[c]	1616 (2)	NH_2 (B)
ν_{68}	1608 ± 2 (38)	1615 ± 1 (32)	1624 (68)	C═O (S) + NH_2 (B)

	in CH_3OH[a]	in CD_3OD[a]	*m*-ABDI—OH^+ in CH_3OH	
Species B				
ν_{65}	n.d.[c]	1501 ± 6 (32)	1507 (51)	Ph (S) + NH_2 (B) + C═C—H (e-B) + C—O—H (B)
ν_{66}	1513 ± 4 (52)	1512 ± 4 (18)	1512 (49)	C═O (S) + C═N (S) + Ph (S) + C—CH_3 (B) + N—CH_3 (B) + C—O—H (B)
ν_{67}	1532 ± 2 (100)	1528 ± 1 (100)	1526 (76)	C═C (e-S) + Ph (S) + C═C—H (e-B)
ν_{68}	1554 ± 3 (87)	1553 ± 1 (44)	1553 (100)	C═N (S) + C—N (S) + C—CH_3 (B) + N—CH_3 (B)
ν_{69}	1592 ± 2 (28)	1596 ± 1 (18)	1592 (63)	Ph (S) + C═C—H (e-B)
ν_{70}			1618 (66)	NH_2 (B)

[a]Relative intensities normalized to the absorption band near 1530 cm^{-1} are listed in parentheses. [b]Vibrational wavenumbers calculated with TD-B3LYP/6-31G* are scaled by 0.96. [c]n.d. = not determined.

cm^{-1} in CD_3OD (Figure 7b). The EADS obtained for *m*-ABDI in CH_3OH and CD_3OD are shown in Figure 8c and e, with associated evolution curves shown in Figure 8d and f, respectively. In both solvents, the positive features of the black curves (species A) exhibit a single exponential decay of time constant ~16 ps. The positive features of the red curves (species B) are characteristic of an intermediate with a rise time constant of ~16 ps in both CH_3OH and CD_3OD and a decay constant of ~58 ps in CH_3OH and ~247 ps in CD_3OD.

The observed positive features of the black curves (species A) in Figure 8a, c, and e were deconvoluted, and the data are shown in Table 2. The deconvoluted spectra of these features in the three solvents are shown in Figure S12 (Supporting Information). In CD_3CN, four bands at 1513 ± 13, 1531 ± 5, 1557 ± 1, and 1613 ± 1 cm^{-1} with relative intensities 51:100:74:27 were observed. The deconvoluted bands in CH_3OH are at 1512 ± 4, 1531 ± 3, 1560 ± 2, and 1608 ± 2 cm^{-1} with relative intensities 33:100:103:38. Similar bands and relative intensities (in parentheses) at 1515 ± 3 (37), 1530 ± 2 (100), 1557 ± 1 (100), and 1615 ± 1 (32) cm^{-1} were observed in CD_3OD; additional features at 1414 ± 2, 1434 ± 1, 1471 ± 2, and 1500 ± 9 were also observed because of less interference by the solvent in this spectral region.

To characterize the nature of the observed bands for species A, we performed TDDFT optimizations on the first electronically excited state of *m*-ABDI in CH_3CN and CH_3OH at the B3LYP/6-31G* level with the incorporation of the influence of the solvent by applying a polarizable-continuum model (PCM). The calculated results (Table 2 and Figure 9a and b) agree satisfactorily with the observed new features in terms of wavenumbers and relative intensities. The observed features at 1513, 1531, 1557, and 1613 cm^{-1} correspond to 1507, 1512, 1557, and 1624 cm^{-1} predicted by TDDFT. We thus conclude that these new features are due to IR absorption of the S_1 state of *m*-ABDI. Accordingly, the observed TA band at 1613 cm^{-1} in CD_3CN is assignable to the C═O stretching coupled with the NH_2 bending mode (calculated at 1624 cm^{-1}) of the S_1 state (Figures S13 and S14, Supporting Information). That the wavenumbers of the C═O stretching mode are smaller in the excited state than in the ground state (1710 cm^{-1}) is attributed to the decreased double-bond character of the carbonyl in S_1.

We deconvoluted the absorption features of the intermediate observed in CH_3OH (red curves in Figure 8c) into four bands at 1513 ± 4, 1532 ± 2, 1554 ± 3, and 1592 ± 2 cm^{-1}, with relative intensities 52:100:87:28. Similar bands at 1512 ± 4, 1528 ± 1, 1553 ± 1, and 1596 ± 1 cm^{-1} were observed for *m*-ABDI in CD_3OD; additional features at 1415 ± 3, 1433 ± 1, 1475 ± 2, and 1501 ± 6 cm^{-1} were also observed because of less interference by the solvent in this spectral region. In general, the spectrum of this intermediate species is similar to that of the S_1 state of *m*-ABDI except some spectral shifts; the band near 1608 cm^{-1} disappeared, and the band near 1592 cm^{-1} is enhanced and becomes isolated. It should be noted that the intensity ratios of overlapped bands for the electronically excited state (black curve in Figure 8) and the intermediate (red curve in Figure 8) might not be as reliable as the isolated bands.

To characterize the nature of these TA bands of the intermediate (species B), we performed TDDFT optimizations on the S_1 state of *m*-ABDI with the SSHB modes shown in Figure 4 and that of protonated species *m*-ABDI−NH^+ and *m*-ABDI−OH^+ (Chart 2), which can be formed via excited-state proton transfer (ESPT). These optimized excited-state SSHB systems are shown in Figure S15 (Supporting Information),

dx.doi.org/10.1021/jp3093397 | J. Phys. Chem. B 2013, 117, 2705−2716

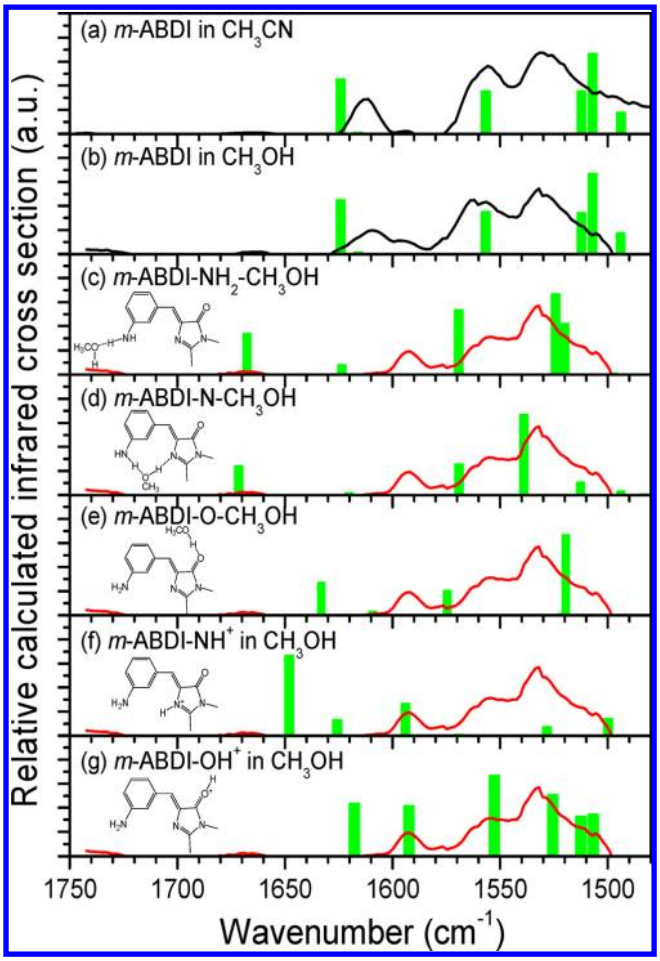

Figure 9. TDDFT-calculated infrared absorption of *m*-ABDI in (a) CH_3CN and (b) CH_3OH, its hydrogen-bonded complexes (c) *m*-ABDI−NH_2−CH_3OH, (d) *m*-ABDI−N−CH_3OH, and (e) *m*-ABDI−O−CH_3OH, and the protonated forms (f) *m*-ABDI−NH^+ and (g) *m*-ABDI−OH^+ in CH_3OH. The EADS of species A in CD_3CN and CH_3OH (black curves in Figure 8a and c) obtained from the global analysis are shown in parts a and b, respectively, and that obtained for species B in CH_3OH (red curve in Figure 8c) is shown in parts c−g for comparison. All the vibration intensities (green bars) are normalized with respect to the most intense peak in the region 1480−1750 cm^{-1}.

Chart 2

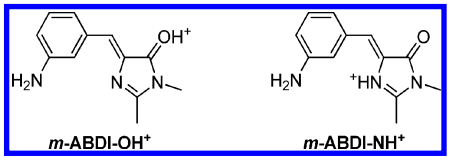

and the vibration modes are depicted in Figures S16−S20 (Supporting Information). A comparison of the TDDFT-predicted and the observed absorption features of the intermediate are depicted in Figure 9c−g. As the hydrogen-bonded species shown in Figure 4 represent only some possible SSHB forms for *m*-ABDI in CH_3OH and each observed TA signal might result from more than one SSHB form, a definitive assignment of the carrier of these bands is difficult. Nevertheless, the calculations provide some indication of a possible origin of the observed TA signals of the intermediate. Regarding the new species, the two candidates *m*-ABDI−OH^+ and *m*-ABDI−NH^+ have predicted bands similar to observations, with a unique band near 1592 cm^{-1}. However, the formation of *m*-ABDI−NH^+ is less likely than that of *m*-ABDI−OH^+ because an intense band near 1648 cm^{-1} that corresponds to the C═O stretching mode was predicted for the former but unobserved (Figure 9f). Recall that the C═O stretching in S_1 is at 1608 cm^{-1} (Figure 9b) and this band disappears upon the formation of the intermediate. The unique feature near 1592 cm^{-1} might correspond to the phenyl and the exocyclic C═C stretching modes of *m*-ABDI−OH^+ (Table 2). The excited state *m*-ABDI−OH^+ is likely formed via ESPT from CH_3OH to *m*-ABDI.

Excited-State Relaxation Mechanism. The observation that $\Phi_f + 2\Phi_{ZE} \cong 1.0$ for *m*-ABDI in aprotic solvents[16] conforms to the OBF mechanism for *E,Z*-photoisomerization of alkenes, in which the IC occurs from a perpendicular $^1p^*$ state and the probability of partition to the *E* and *Z* isomers is equal. The fluorescence decay time ∼7.9 ns for *m*-ABDI in CD_3CN is about 10 000 times that for *p*-ABDI (0.3−1.0 ps), which indicates that the τ torsion in the excited state encounters a significant barrier. This phenomenon is similar to that observed for *meta*- and *para*-aminostilbenes, which was dubbed as the *meta*-amino effect.[4−6] In analogy to the cases of *trans*-aminostilbenes,[6,38−40,52,53] a large τ-torsion barrier for *m*-ABDI might result from a lower energy for the *Z** vs $^1p^*$ state. Compared to the *Z** and $^1p^*$ states of *p*-ABDI, the energy of the *Z** state should be lowered and that of the $^1p^*$ state should be raised in the case of *m*-ABDI because of a stronger charge-transfer character for the *Z** and less mesomeric stabilization of the $^1p^*$ state by the amino group. As estimated with the fluorescence maxima (578 vs 469 nm) in CH_3CN, the *Z** state of *m*-ABDI is lower by 11.5 kcal mol^{-1} than that of *p*-ABDI. The dark $^1p^*$ state does not provide an emission signal for direct evaluation of the energy difference of the $^1p^*$ state in *m*-ABDI vs *p*-ABDI. It was reported to be ∼7 kcal mol^{-1} higher for the $^1p^*$ state of *trans*-3-aminostilbene than that of *trans*-4-aminostilbene.[6] A similar size might be expected for the case of *m*-ABDI vs *p*-ABDI. Although the relative energies of the *Z** and $^1p^*$ states of *p*-ABDI are unknown and the *Z** → $^1p^*$ process should be exergonic, the simultaneous stabilization of *Z** and destabilization of $^1p^*$ on going from *p*-ABDI to *m*-ABDI with a total energy change near 19 kcal mol^{-1} should render the *Z** → $^1p^*$ process of *m*-ABDI endergonic with a significant barrier. In addition to a slower rate for the τ torsion, another contribution to the longer fluorescence lifetime of *m*-ABDI vs *p*-ABDI is the less allowed $S_1 \rightarrow S_0$ transition (*vide supra*). On the basis of Φ_f (0.16) and τ_f (7.9 ns), the time constants of the radiative process (τ_f/Φ_f) and of the nonradiative relaxation through the τ torsion ($\tau_f/(1 - \Phi_f)$) of *m*-ABDI in CH_3CN are ∼50 and ∼10 ns, respectively (Figure 10a).

The rapid fluorescence quenching (∼16 and 62 ps) and the small Φ_{ZE} (0.08) for *m*-ABDI in CH_3OH indicate that the nonradiative decay in CH_3OH differs from that in CD_3CN and is strongly affected by the SSHB interactions. A simplified scheme for the decay dynamics is shown in Figure 10b, where the HB in the labels denotes the presence of hydrogen bonding with the solvent molecules. The presence of an intermediate excited state (ESPT*) that is formed via ESPT is proposed on the basis of the observation of a rise time of ∼16 ps and a decay time of ∼58 ps for the species B in the global analysis of TRIR spectra. An alternative explanation of the intermediate excited state is a HB-associated TICT state.[9,54,55] However, the dynamics of a HB-associated TICT state are generally more

dx.doi.org/10.1021/jp3093397 | J. Phys. Chem. B 2013, 117, 2705−2716

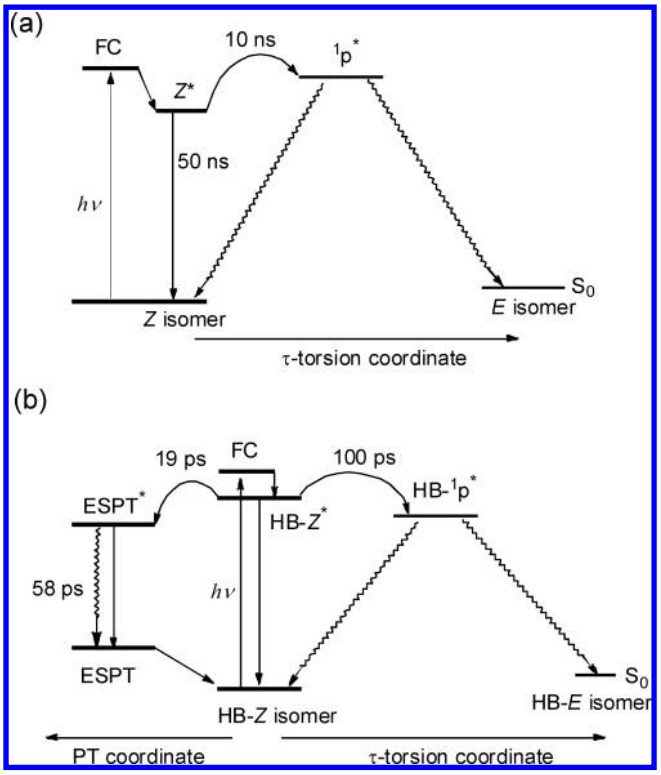

Figure 10. Schematic representation of the proposed excited-state relaxation dynamics for *m*-ABDI in (a) CH_3CN and (b) CH_3OH. The HB and PT in the labels denote hydrogen-bonded and proton transfer, respectively.

complicated than a simple rise and decay observed herein.[55−57] The finite but non-negligible Φ_{ZE} indicates that the barrier for the τ torsion is significantly less for *m*-ABDI in CH_3OH than in CH_3CN. Assuming that the quantum yield for the τ torsion is equal to $2\Phi_{ZE}$ (i.e., 0.16), the fluorescence decay time ∼16 ps for HB-*Z** suggests a decay time coefficient of ∼100 ps ($((0.16 \times 16^{-1})^{-1})$ for the τ torsion from HB-*Z** to HB-^{1}p*. Accordingly, the time coefficient for the HB-*Z** → ESPT* transition is 19 ps ($(((16)^{-1} - (100)^{-1})^{-1})$. We also performed the target analysis[28,51] with this dynamic model

$$A \xrightarrow{k_1} B \xrightarrow{k_2} C,\ A \xrightarrow{k_3} C$$

(species A, B, and C represent the HB-*Z**, ESPT*, and HB-*Z*, respectively, in Figure 10b) by assuming that the HB-^{1}p* state is a dark state and the formation time constant of the HB-^{1}p* state is 100 ps. We obtained a rise time constant of 18.7 ± 0.3 ps and a decay constant of 57.6 ± 0.3 ps for the ESPT* state. The difference between the rise time of ∼16 ps of ESPT* obtained from the global fitting and the rise time of ∼19 ps obtained from the target fitting is within experimental uncertainties. The EADS obtained from this dynamic model do not change from the previous one

$$A \xrightarrow{k_1} B \xrightarrow{k_2} C$$

because there was no additional bright state in this model (Figure S21, Supporting Information). Although the τ-torsion and the ESPT processes are depicted as independent decay channels in Figure 10b, we cannot exclude the possibility that the two processes couple with one another in the early stage of the τ torsion (i.e., τ-torsion-induced proton transfer) and the isomerization is aborted when the intermediate ESPT* is formed.

According to the TDDFT calculations, the protonated site is likely on the carbonyl oxygen, corresponding to *m*-ABDI−OH^+ (Chart 2). The occurrence of ESPT to the carbonyl oxygen is consistent with our recent conclusion with a series of derivatives of *m*-ABDI containing site-specific intramolecular HBs either to the carbonyl oxygen or to the imino nitrogen.[37] The occurrence of ESPT from the solvent to the imidazolinone carbonyl was also proposed for *meta*-methoxybenzylidenedimethylimidazolinone, a *meta*-methoxy derivative of *p*-HBDI (*m*-MeOBDI), in CH_3OH/H_2O (1/9) at pH 5.5.[58] The rise time 0.9 ps and decay constant 25 ps for *m*-MeOBDI are both smaller than those of *m*-ABDI, which is attributed to different solvent conditions.

The time constant for the τ torsion decreased by 100 times from CH_3CN (10 ns) to CH_3OH (100 ps), indicating that the τ-torsion barrier is decreased significantly by the SSHB interactions. With the same concept discussed above, a decreased τ-torsion barrier can occur provided that the SSHB interactions stabilize the ^{1}p* state much more than the *Z** state (i.e., HB-^{1}p* is lower in energy than HB-*Z**).

The SSHB effect on the excited-state dynamics of *m*-ABDI differs significantly from that of the *para* isomer *p*-ABDI, for which ESPT does not occur and for which only the PES of the τ torsion is perturbed.[19] According to the scenario of Figure 10b, the absence of ESPT for *p*-ABDI could be attributed to the ultrafast decay (∼1 ps) of the excited state via the τ torsion so that the ESPT process cannot compete with the τ torsion. The *meta*-amino effect in *m*-ABDI raises the torsion barrier and slows the τ torsion. The time constant 100 ps for the τ torsion of *m*-ABDI in CH_3OH is much larger than that (19 ps) for the ESPT process. It should also be noted that the driving force for the ESPT process is inherently larger in *m*-ABDI vs *p*-ABDI, as the former possesses a stronger charge-transfer character and thus a better hydrogen-bond acceptor of the carbonyl oxygen.

The rapid fluorescence intensity decay for the initial 10 ps (Figure 6) deserves a comment. Both HB-*Z** and ESPT* are fluorescent, and their decay coefficients ∼16 and ∼62 ps match well with the decay constants ∼16 and 58 ps derived from global fitting of the TRIR spectra. The rapid fluorescence decay in the first 10 ps has no corresponding component in the TRIR spectra, indicating that this decay does not involve HB-*Z** or ESPT*. The rapid decay occurred during the period when solvent-induced vibrational relaxation and solvation were taking place so that interpretation of this relaxation process becomes complex. Nevertheless, it is possible that the molecular conformation and electronic character of *m*-ABDI in the excited state was significantly affected by SSHB in a way that the optical transition probability is much lower for the relaxed electronic excited state (HB-*Z**) than for the Franck−Condon state (FC) to account for the ∼60% decrease in total fluorescence intensities in the first 10 ps. Another possibility is that the FC state with higher energy might overcome the τ-torsion barrier more readily than the HB-*Z** state. However, as is the situation of the SSHB effect on the PES along the τ-torsion coordinate for *p*-ABDI,[26] the τ torsion is aborted in an early stage (i.e., at small τ-torsion angles), so that the observed Z → *E* isomerization quantum yield (0.08) is much lower than a total quantum yield of ∼0.60 for the τ torsion. In this case, the rate for HB-Z* → ESPT* might be just ∼16 ps and the rate of HB-*Z** → HB-^{1}p* could be much greater than 100 ps, with the

dx.doi.org/10.1021/jp3093397 | J. Phys. Chem. B 2013, 117, 2705−2716

total decay of HB-Z* ~16 ps. Further experiments are needed to confirm such a possibility.

Finally, it deserves a comparison of the *meta*-NH_2 and the *meta*−OH effect[58,59] on the excited-state dynamics of GFP chromophores. The *meta*-OH isomer *m*-HBDI was shown to display fluorescence decay times up to 30 times longer than *p*-HBDI does in CH_3CN. Such a *meta*-OH effect is much less significant as compared to the *meta*-NH_2 effect, which induces a 10^4 times increase in the fluorescence lifetime. The smaller *meta*-OH vs *meta*-NH_2 effect can be attributed to a smaller increase in the barrier for the τ torsion. We reasoned that the hydroxyl group is a weaker donor than the amino group so that the stabilization of the *Z** state and the destabilization of the ^{1}p* state on going from *p*-HBDI to *m*-HBDI are to a much weaker extent than the *meta*-NH_2 effect. Similar behavior was found for the comparison of *trans*-3-hydroxystilbenes[60−62] and *trans*-3-aminostilbenes.[6,36,39] For anionic *m*-HBDI, the stronger oxido (O^-) donor does lead to a feature of band splitting in the electronic absorption spectrum similar to the case of the *meta*-NH_2 effect.[59] This phenomenon would in principle significantly raise the τ-torsion barrier as is the *meta*-NH_2 effect. However, the solvent condition of CH_3OH/H_2O (1/9) and pH 11.5 required for the formation of anionic *m*-HBDI in the ground state also introduces SSHB interactions and ultrafast ESPT processes, which counterbalances the substituent effect.

CONCLUSION

The excited decay dynamics for *m*-ABDI in CD_3CN, CH_3OH, and CD_3OD have been investigated with femtosecond fluorescence and transient IR absorption spectroscopy. In CD_3CN, the decays are mainly through the fluorescence and the exocyclic C=C bond (τ) torsion. Because of a slow rate (10 ns) of the τ torsion, the observed Φ_f (0.16) is exceptionally large among the unconstrained GFP chromophores known in nonviscous solvents. In CH_3OH, the participation of SSHB strongly affects the decay mechanism, as evidenced by the small Φ_{ZE} (0.08) and Φ_f ($<10^{-3}$). There exists a fluorescent intermediate state (ESPT*), which was not observed in the case of the *para* isomer *p*-ABDI. The ESPT* is likely due to ESPT from CH_3OH to the carbonyl oxygen of *m*-ABDI. The SSHB interactions might also couple with the τ torsion to decrease the barrier and/or to initiate the ESPT. That the SSHB effects on the decay dynamics are larger for *m*-ABDI than for *p*-ABDI is attributed to a stronger charge-transfer character and a larger barrier for the τ torsion of the S_1 state. These results indicate the importance of not only SSHB but also the location of substituents on the excited decay dynamics of a GFP-like chromophore. These results provide useful information for structural engineering toward highly fluorescent GFP chromophores.

ASSOCIATED CONTENT

Supporting Information

Deconvoluted IR spectrum of *m*-ABDI in selected solvents, fluorescence decay profiles, time-dependent frequencies, fitting of decay profiles, TDDFT-optimized geometries of hydrogen-bonded complexes, TDDFT-calculated infrared absorption, EADS from target analysis and TRES of *m*-ABDI in CH_3OH, table of optimized structures and relative energies of *m*-ABDI and associated complexes, tables of calculated vibrational modes, complete ref 29, and Cartesian coordinates of *m*-ABDI and its hydrogen-bonded complexes in their electronically excited and ground states. This material is available free of charge via the Internet at http://pubs.acs.org.

AUTHOR INFORMATION

Corresponding Author

*Phone: (+886)35131459 (Y.-P.L.); (+886)35131524 (E.W.-G.D.); (+886)233661649 (J.-S.Y.). E-mail: yplee@mail.nctu.edu.tw (Y.-P.L.); diau@mail.nctu.edu.tw (E.W.-G.D.); jsyang@ntu.edu.tw (J.-S.Y.).

Notes

The authors declare no competing financial interest.

ACKNOWLEDGMENTS

National Science Council of Taiwan (Grant Nos. NSC100-2745-M-009-001-ASP and NSC98-2119-M-002-008-MY3) and the Ministry of Education, Taiwan ("Aim for the Top University Plan" of NCTU and the Excellent Research Project 10R80912-3 of NTU) supported this work. The National Center for High-Performance Computing and the Computing Center of NTU provided computer time. We thank Dr. Chao-Ping Hsu at the Institute of Chemistry of Academia Sinica for helpful discussions.

REFERENCES

(1) Zimmerman, H. E. *Meta-ortho* Effect in Organic Photochemistry: Mechanistic and Exploratory Organic Photochemistry. *J. Phys. Chem. A* **1998**, *102*, 5616−5621.

(2) Wang, P.; Hu, H.; Wang, Y. Application of the Excited State Meta Effect in Photolabile Protecting Group Design. *Org. Lett.* **2007**, *9*, 2831−2833.

(3) Bouchoux, G.; Sablier, M.; Miyakoshi, T.; Honda, T. A '*meta* Effect' in the Fragmentation Reactions of Ionised Alkyl Phenols and Alkyl Anisoles. *J. Mass Spectrom.* **2012**, *47*, 539−546.

(4) Thompson, A. L.; Ahn, T.-S.; Thomas, K. R. J.; Thayumanavan, S.; Martínez, T. J.; Bardeen, C. J. Using *meta* Conjugation to Enhance Charge Separation versus Charge Recombination in Phenylacetylene Donor−Bridge−Acceptor Complexes. *J. Am. Chem. Soc.* **2005**, *127*, 16348−16349.

(5) Gaab, K. M.; Thompson, A. L.; Xu, J.; Martínez, T. J.; Bardeen, C. J. *Meta*-Conjugation and Excited-State Coupling in Phenylacetylene Dendrimers. *J. Am. Chem. Soc.* **2003**, *125*, 9288−9289.

(6) Lewis, F. D.; Kalgutkar, R. S.; Yang, J.-S. The Photochemistry of *trans-ortho-*, *-meta-*, and *-para*-Aminostilbenes. *J. Am. Chem. Soc.* **1999**, *121*, 12045−12053.

(7) Chalfie, M.; Tu, Y.; Euskirchen, G.; Ward, W.; Prasher, D. Green Fluorescent Protein as a Marker for Gene Expression. *Science* **1994**, *263*, 802−805.

(8) Zimmer, M. Green Fluorescent Protein (GFP): Applications, Structure, and Related Photophysical Behavior. *Chem. Rev.* **2002**, *102*, 759−781.

(9) Remington, S. J. Green Fluorescent Protein: A Perspective. *Protein Sci.* **2011**, *20*, 1509−1519.

(10) Weber, W.; Helms, V.; McCammon, J. A.; Langhoff, P. W. Shedding Light on the Dark and Weakly Fluorescent States of Green Fluorescent Proteins. *Proc. Natl. Acad. Sci. U.S.A.* **1999**, *96*, 6177−6182.

(11) Paige, J. S.; Wu, K. Y.; Jaffrey, S. R. RNA Mimics of Green Fluorescent Protein. *Science* **2011**, *333*, 642−646.

(12) You, Y.; He, Y.; Burrows, P. E.; Forrest, S. R.; Petasis, N. A.; Thompson, M. E. Fluorophores Related to the Green Fluorescent Protein and Their Use in Optoelectronic Devices. *Adv. Mater.* **2000**, *12*, 1678−1681.

(13) Chuang, W.-T.; Chen, B.-S.; Chen, K.-Y.; Hsieh, C.-C.; Chou, P.-T. Fluorescent Protein Red Kaede Chromophore; One-Step, High-Yield Synthesis and Potential Application for Solar Cells. *Chem. Commun.* **2009**, 6982−6984.

(14) Niwa, H.; Inouye, S.; Hirano, T.; Matsuno, T.; Kojima, S.; Kubota, M.; Ohashi, M.; Tsuji, F. I. Chemical Nature of the Light Emitter of the Aequorea Green Fluorescent Protein. *Proc. Natl. Acad. Sci. U.S.A.* **1996**, *93*, 13617−13622.
(15) Kojima, S.; Ohkawa, H.; Hirano, T.; Maki, S.; Niwa, H.; Ohashi, M.; Inouye, S.; Tsuji, F. I. Fluorescent Properties of Model Chromophores of Tyrosine-66 Substituted Mutants of Aequorea Green Fluorescent Protein (GEP). *Tetrahedron Lett.* **1998**, *39*, 5239−5242.
(16) Yang, J.-S.; Huang, G.-J.; Liu, Y.-H.; Peng, S.-M. Photoisomerization of the Green Fluorescence Protein Chromophore and the *meta*- and *para*-Amino Analogues. *Chem. Commun.* **2008**, 1344−1346.
(17) Meech, S. R. Excited State Reactions in Fluorescent Proteins. *Chem. Soc. Rev.* **2009**, *38*, 2922−2934.
(18) Tolbert, L. M.; Baldridge, A.; Kowalik, J.; Solntsev, K. M. Collapse and Recovery of Green Fluorescent Protein Chromophore Emission through Topological Effects. *Acc. Chem. Res.* **2012**, *45*, 171−181.
(19) Wu, L.; Burgess, K. Syntheses of Highly Fluorescent GFP-Chromophore Analogues. *J. Am. Chem. Soc.* **2008**, *130*, 4089−4096.
(20) Baranov, M. S.; Lukyanov, K. A.; Borissova, A. O.; Shamir, J.; Kosenkov, D.; Slipchenko, L. V.; Tolbert, L. M.; Yampolsky, I. V.; Solntsev, K. M. Conformationally Locked Chromophores as Models of Excited-State Proton Transfer in Fluorescent Proteins. *J. Am. Chem. Soc.* **2012**, *134*, 6025−6032.
(21) Ivashkin, P. E.; Yampolsky, I. V.; Lukyanov, K. A. Synthesis and Properties of Chromophores of Fluorescent Proteins. *Russ. J. Bioog. Chem.* **2009**, *35*, 652−669.
(22) Chen, K.-Y.; Cheng, Y.-M.; Lai, C.-H.; Hsu, C.-C.; Ho, M.-L.; Lee, G.-H.; Chou, P.-T. *Ortho* Green Fluorescence Protein Synthetic Chromophore; Excited-State Intramolecular Proton Transfer via a Seven-Membered-Ring Hydrogen-Bonding System. *J. Am. Chem. Soc.* **2007**, *129*, 4534−4535.
(23) Huang, G.-J.; Yang, J.-S. The *N*-Arylamino Conjugation Effect in the Photochemistry of Fluorescent Protein Chromophores and Aminostilbenes. *Chem. Asian J.* **2010**, *5*, 2075−2085.
(24) Petkova, I.; Dobrikov, G.; Banerji, N.; Duvanel, G.; Perez, R.; Dimitrov, V.; Nikolov, P.; Vauthey, E. Tuning the Excited-State Dynamics of GFP-Inspired Imidazolone Derivatives. *J. Phys. Chem. A* **2010**, *114*, 10−20.
(25) Voliani, V.; Bizzarri, R.; Nifosi, R.; Abbruzzetti, S.; Grandi, E.; Viappiani, C.; Beltram, F. *Cis-trans* Photoisomerization of Fluorescent-Protein Chromophores. *J. Phys. Chem. B* **2008**, *112*, 10714−10722.
(26) Huang, G.-J.; Cheng, C.-W.; Hsu, H.-Y.; Prabhakar, Ch.; Lee, Y.-P.; Diau, E. W.-G.; Yang, J.-S. Effects of Hydrogen Bonding on Internal Conversion of GFP-like Chromophores. I. The *para*-Amino Systems. *J. Phys. Chem. B* **2013**, DOI: 10.1021/jp3093379.
(27) van Stokkum, I. H. M.; Larsen, D. S.; van Grondelle, R. Global and Target Analysis of Time-Resolved Spectra. *Biochim. Biophys. Acta* **2004**, *1657*, 82−104.
(28) Snellenburg, J. J.; Laptenok, S. P.; Seger, R.; Mullen, K. M.; van Stokkum, I. H. M. Glotaran: A Java-Based Graphical User Interface for the R Package TIMP. *J. Stat. Softw.* **2012**, *49*, 1−22.
(29) Frisch, M. J.; Trucks, G. W.; Schlegel, H. B.; Scuseria, G. E.; Robb, M. A.; Cheeseman, J. R.; Scalmani, G.; Barone, V.; Mennucci, B.; Petersson, G. A.; et al.; Gaussian, Inc.: Wallingford, CT, 2009.
(30) Becke, A. D. Density-Functional Thermochemistry. III. The Role of Exact Exchange. *J. Chem. Phys.* **1993**, *98*, 5648−5652.
(31) Lee, C.; Yang, W.; Parr, R. G. Development of the Colle-Salvetti Correlation-Energy Formula into a Functional of the Electron Density. *Phys. Rev. B* **1988**, *37*, 785−789.
(32) Cances, E.; Mennucci, B.; Tomasi, J. A New Integral Equation Formalism for the Polarizable Continuum Model: Theoretical Background and Applications to Isotropic and Anisotropic Dielectrics. *J. Chem. Phys.* **1997**, *107*, 3032−3041.
(33) Foresman, J. B.; Frisch, Æ. *Exploring Chemistry with Electronic Structure Methods*, 2nd ed.; Gaussian, Inc.: Pittsburgh, PA, 1996.
(34) Scott, A. P.; Radom, L. Harmonic Vibrational Frequencies: An Evaluation of Hartree−Fock, Møller−Plesset, Quadratic Configuration Interaction, Density Functional Theory, and Semiempirical Scale Factors. *J. Phys. Chem.* **1996**, *100*, 16502−16513.
(35) Andersson, M. P.; Uvdal, P. New Scale Factors for Harmonic Vibrational Frequencies Using the B3LYP Density Functional Method with the Triple-ζ Basis Set 6-311+G(d,p). *J. Phys. Chem. A* **2005**, *109*, 2937−2941.
(36) Lewis, F. D.; Weigel, W. Excited state properties of Donor-acceptor Substituted *trans*-Stilbenes: The *meta*-Amino Effect. *J. Phys. Chem. A* **2000**, *104*, 8146−8153.
(37) Huang, G.-J.; Ho, J.-H.; Prabhakar, Ch.; Liu, Y.-H.; Peng, S.-M.; Yang, J.-S. Site-Selective Hydrogen-Bonding-Induced Fluorescence Quenching of Highly Solvatofluorochromic GFP-like Chromophores. *Org. Lett.* **2012**, *14*, 5034−5037.
(38) Yang, J.-S.; Chiou, S.-Y.; Liau, K.-L. Fluorescence Enhancement of *trans*-4-Aminostilbene by *N*-phenyl Substitutions: The "Amino Conjugation Effect". *J. Am. Chem. Soc.* **2002**, *124*, 2518−2527.
(39) Yang, J.-S.; Liau, K.-L.; Tu, C.-W.; Hwang, C.-Y. Excited-State Behavior of *N*-Phenyl-Substituted *trans*-3-Aminostilbenes: Where the "*m*-Amino Effect" Meets the "Amino-Conjugation Effect". *J. Phys. Chem. A* **2005**, *109*, 6450−6456.
(40) Yang, J.-S.; Liau, K.-L.; Li, C.-Y.; Chen, M.-Y. *Meta* Conjugation Effect on the Torsional Motion of Aminostilbenes in the Photo-induced Intramolecular Charge-Rransfer State. *J. Am. Chem. Soc.* **2007**, *129*, 13183−13192.
(41) Rafiq, S.; Rajbongshi, B. K.; Nair, N. N.; Sen, P.; Ramanathan, G. Excited State Relaxation Dynamics of Model Green Fluorescent Protein Chromophore Analogs: Evidence for *cis*−*trans* Isomerism. *J. Phys. Chem. A* **2011**, *115*, 13733−13742.
(42) Banno, M.; Ohta, K.; Tominaga, K. Ultrafast Vibrational Dynamics and Solvation Complexes of Methyl Acetate in Methanol Studied by Sub-Picosecond Infrared Spectroscopy. *J. Raman Spectrosc.* **2008**, *39*, 1531−1537.
(43) Banno, M.; Ohta, K.; Yamaguchi, S.; Hirai, S.; Tominaga, K. Vibrational Dynamics of Hydrogen-Bonded Complexes in Solutions Studied with Ultrafast Infrared Pump−Probe Spectroscopy. *Acc. Chem. Res.* **2009**, *42*, 1259−1269.
(44) Hirai, S.; Banno, M.; Ohta, K.; Palit, D. K.; Tominaga, K. Vibrational Dynamics of the CO Stretching Mode of 9-Fluorenone in Alcohol Solution. *Chem. Phys. Lett.* **2007**, *450*, 44−48.
(45) In order to determine the spectral frequencies, the time-resolved spectra for each time delay were fit to a log-normal line shape function[46]

$$g(\nu) = h \exp\left\{-\ln(2)\left(\frac{\ln[1 + 2b(\nu - \nu_p)/\Delta]}{b}\right)^2\right\}$$

where h, ν_p, Δ, and b are the peak height, frequency, width, and asymmetry parameter, respectively.
(46) Fraser, R. D. B.; Suzuki, E. In *Spectral Analysis*; Blackburn, J. A., Ed.; Marcel Dekker: New York, 1970; p 171.
(47) Maroncelli, M.; Fleming, G. R. Picosecond Solvation Dynamics of Coumarin 153: The Importance of Molecular Aspects of Solvation. *J. Chem. Phys.* **1987**, *86*, 6221−6239.
(48) Sension, R. J.; Kobayashi, T.; Strauss, H. L. Comparison of Experiment and Theory for the Resonance Raman Spectrum of I_2 in Solution. II. The Raman Excitation and Depolarization Profiles in *n*-Hexane. *J. Chem. Phys.* **1987**, *87*, 6221−6232.
(49) Horng, M. L.; Gardecki, J. A.; Papazyan, A.; Maroncelli, M. Subpicosecond Measurements of Polar Solvation Dynamics: Coumarin 153 Revisited. *J. Phys. Chem.* **1995**, *99*, 17311−17337.
(50) The estimated total intensity was calculated with the equation below.[46]

$$I(t) = \left(\frac{\pi}{4\ln(2)}\right)^{1/2} h(t)\Delta(t) \exp\left(\frac{b^2}{4\ln(2)}\right)$$

(51) van Stokkum, I. H. M.; Larsen, D. S.; van Grondelle, R. Global and Target Analysis of Time-Resolved Spectra. *Biochim. Biophys. Acta* **2004**, *1657*, 82−104.
(52) Yang, J.-S.; Laiu, K.-L.; Wang, C.-M.; Hwang, C.-Y. Substituent-Dependent Photoinduced Intramolecular Charge Rransfer in *N*-Aryl-Substituted *trans*-4-Aminostilbenes. *J. Am. Chem. Soc.* **2004**, *126*, 12325−12335.
(53) Yang, J.-S.; Lin, C.-K.; Lahoti, A. M.; Tseng, C.-K.; Liu, Y.-H.; Lee, G.-H.; Peng, S.-M. Effect of Ground-State Twisting on the *trans*→*cis* Photoisomerization and TICT State Formation of Aminostilbene. *J. Phys. Chem. A* **2009**, *113*, 4868−4877.
(54) Dong, J.; Abulwerdi, F.; Baldridge, A.; Kowalik, J.; Solntsev, K. M.; Tolbert, L. M. Isomerization in Fluorescent Protein Chromophores Involves Addition/Elimination. *J. Am. Chem. Soc.* **2008**, *130*, 14096−14098.
(55) Kwok, W.-M.; George, M. W.; Grills, D. C.; Ma, C.; Matousek, P.; Parker, A. W.; Phillips, D.; Toner, W. T.; Towrie, M. Direct Observation of a Hydrogen-Bonded Charge-Transfer State of 4-Dimethylaminobenzonitrile in Methanol by Time-Resolved IR Spectroscopy. *Angew. Chem., Int. Ed. Engl.* **2003**, *42*, 1826−1830.
(56) Kwok, W. M.; Ma, C.; George, M. W.; Grills, D. C.; Matousek, P.; Parker, A. W.; Phillips, D.; Toner, W. T.; Towrie, M. Solvent Effects on the Charge Transfer Excited States of 4-Dimethylaminobenzonitrile (DMABN) and 4-Dimethylamino-3,5-Dimethylbenzonitrile (TMABN) Studied by Time-Resolved Infrared Spectroscopy: A Direct Observation of Hydrogen Bonding Interactions. *Photochem. Photobiol. Sci.* **2007**, *6*, 987−994.
(57) Zhao, G.-J.; Han, K.-L. Time-Dependent Density Functional Theory Study on Hydrogen-Bonded Intramolecular Charge-Transfer Excited State of 4-Dimethylamino-Benzonitrile in Methanol. *J. Comput. Chem.* **2008**, *29*, 2010−2017.
(58) Solntsev, K. M.; Poizat, O.; Dong, J.; Rehault, J.; Lou, Y.; Burda, C.; Tolbert, L. M. *Meta* and *para* Effects in the Ultrafast Excited-State Dynamics of the Green Fluorescent Protein Chromophores. *J. Phys. Chem. B* **2008**, *112*, 2700−2711.
(59) Dong, J.; Solntsev, K. M.; Poizat, O.; Tolbert, L. M. The *meta*-Green Fluorescent Protein Chromophore. *J. Am. Chem. Soc.* **2007**, *129*, 10084−10085.
(60) Lewis, F. D.; Crompton, E. M. Hydroxystilbene Isomer-Specific Photoisomerization versus Proton Transfer. *J. Am. Chem. Soc.* **2003**, *125*, 4044−4045.
(61) Crompton, E. M.; Lewis, F. D. Positional Effects of the Hydroxy Substituent on the Photochemical and Photophysical Behavior of 3- and 4-Hydroxystilbene. *Photochem. Photobiol. Sci.* **2004**, *3*, 660−668.
(62) Lewis, F. D.; Sinks, L. E.; Weigel, W.; Sajimon, M. C.; Crompton, E. M. Ultrafast Proton Transfer Dynamics of Hydroxystilbene Photoacids. *J. Phys. Chem. A* **2005**, *109*, 2443−2451.